A parametric study of the hydrophobicity of rough surfaces based on finite element computations

Muhammad Osman and Roger A. Sauer [1]

Aachen Institute for Advanced Study in Computational Engineering Science (AICES), RWTH Aachen University, Templergraben 55, 52056 Aachen, Germany

Published[2] in *Colloids and Surfaces A: Physicochemical and Engineering Aspects*,
DOI: 10.1016/j.colsurfa.2014.07.029
Submitted on 25 April 2014, Revised on 17 July 2014, Accepted on 21 July 2014

Abstract

Several biological and artificial hydrophobic surfaces exhibit self-cleaning mechanisms, which ensure smooth sliding/rolling of liquid droplets, allowing them to sweep pollutant particles away from the surface. While enhancing of the self-cleaning property is a major topic in numerous industrial applications, the underlying physics is not yet fully understood. The first step towards analyzing this mechanism is studying the surface hydrophobicity, which is characterized by the contact angle and surface topography. In this article, we investigate the wetting of hydrophobic surfaces at three different length-scales, over a range of surface and droplet parameters. A mathematical model describing multi-scale surface topographies is presented, using exponential functions. The contact between liquid droplets and these surfaces is numerically studied using a finite element (FE) droplet model. The introduced models are verified numerically and experimentally. Numerical examples are shown for axisymmetric droplets of different size on surfaces with various contact angles and various levels of surface roughness, representing different length-scales. The corresponding wetted area is computed in order to evaluate the hydrophobicity of the surface. Significant differences are observed in contact angles and wetted areas captured at different length-scales. This highlights the importance of the multi-scale structure of hydrophobic surfaces on wetting. Furthermore, the presented work provides guidelines for the design of artificial hydrophobic surfaces.

Keywords: self-cleaning mechanism, contact angle, static wetting, nonlinear finite element analysis, droplet membranes, rough surface contact.

1 Introduction

Some surfaces such as the lotus leaf exhibit self-cleaning effects (also called lotus effects [3]), when water droplets pass over it. The superhydrophobic nature of these surfaces [8] imposes a large contact angle, and therefore minimum contact area, which forces water droplets to form small semi-spherical shapes. This allows water droplets to roll-off the inclined surface and sweep away pollutant particles. The hydrophobicity is highly influenced by the surface topography [9, 14]. Therefore, manipulating surface morphology over different length-scales, has significantly increased the industrial [17, 28, 19, 12] and research interest to this problem.

[1] corresponding author, email: sauer@aices.rwth-aachen.de
[2] This pdf is the personal version of an article whose final publication is available at www.elsevier.com

While studying hydrophobicity of surfaces, it is quite common to consider a system of a liquid droplet in contact with a substrate surface. The first fundamental equation that quantifies the static contact angle of a liquid droplet on a solid flat surface was proposed by Young in 1805 [33]. However, he did not account for surface roughness captured at the microscopic scale. Wenzel [31] extended the Young equation to account for surface roughness, and modeled a droplet in intimate contact with a rough surface (non-composite state). Cassie and Baxter [9] introduced the composite contact state, where air is trapped between the droplet and the rough surface. They observed that the hydrophobicity of the surface is enhanced by increasing the air-surface fraction. Surface properties which influence the wetting state were investigated by Johnson and Dettre [14]. They argued that surfaces of higher roughness are more likely to be in composite state. Kavousanakisa et al. [15] quantified the effect of geometric characteristics of micro-structured solid surfaces on the wetting state, considering single-level roughness. Similar study was performed by Raeesi et al. [21] for tubes of uniform cross-section. On the nano-level, Lee et al. [16] observed that nano-protrusions decrease the contact area between a water droplet and the surface, causing the contact angle to increase considerably, and thus enhance the hydrophobicity. They observed that contact angles change considerably among different length-scales of a multi-scale structured surface. Static and dynamic wetting on nano-topographical surfaces were recently investigated by Ramiasa [22].

An experimental study of drops on inclined surfaces was performed by El-Sherbini et al. [10]. They investigated the geometry of drops on various surfaces, for different inclinations, contact angles, contact lines, volumes, and surface conditions. Callies et al. [7] discuss the recent advances in water repellency, and examine wetting of surfaces, experimentally. While some experimental measurements of wetting areas on small scales are too difficult, or even impossible [11], numerical treatment of the problem provides suitable solutions, especially for complex surface geometries. One of the first numerical formulations for static droplets in contact with flat surfaces was introduced in 1980 by Brown et al. [6, 5]. They computed the membrane shape of a droplet resting on flat surfaces, by solving the Young-Laplace equation, based on the finite element method (FEM). For more general representation of membrane surfaces, differential geometry based formulations were introduced by Steigmann et al. [29], Agrawal and Steigmann [2, 1], and Sauer et. al [27].

Hydrophobicity is influenced by several factors such as surface energy, electro-magneticity [25], surface chemistry [30], surfactants [18], surface topography, contact angle, and droplet size. In this work, we focus on the last three, which are structural aspects, and show how surface and droplet parameters affect the hydrophobicity of surfaces, considering its multi-scale structure. This study serves as the first step to understand self-cleaning mechanisms. We model a static system of a liquid droplet in contact with a rigid substrate surface of three different topographies; flat, single-roughness and two-level-roughness (double-roughness) surfaces. These can be also seen as different resolutions of the same physical surface. The hydrophobicity is evaluated through two parameters: the contact angle and the contact area (wetted area). Due to the local deformation of the droplet membrane at the region of contact with rough surfaces, local and global contact angles are distinguished, depending on the scale at which they are measured. We use the term apparent for global contact angles captured at larger length-scales (e.g. macro-scale) where the rigid surface appears flat, while the term true is used for local contact angles captured locally at the individual asperities of the rigid surface, at high resolutions (similar definition used in [15]). Similarly, we distinguish apparent and true contact areas to describe global and local surface wetting. Based on a developed FE model, we compute the evaluation variables: the apparent contact angle and the true wetting area, for given droplet and surface parameters, which are discussed in Section 4. We investigate superhydrophobic surfaces with true contact angles in the range $140^\circ \leq \theta_{tr} \leq 180^\circ$. Droplets are considered thermodynamically

stable with zero hysteresis, so only the Young-equilibrium contact angle appears.

2 Numerical model

In this section, we present the governing equations describing the two models; liquid droplet model and the rigid surface model. The implementation of the first model using the FEM is discussed in detail by Sauer et al. [27] and Sauer [26]. We use the stabilization scheme for liquid membranes, introduced in [27], with a stabilization parameter $\mu = 0.01$.

2.1 Droplet model

The liquid droplet can be modeled as a structural membrane whose deformation is governed by the Young-Laplace equation, and an internal liquid flow governed by the Stokes equation. Different approaches can be used to solve the two problems. A simple approach is solving the two problems in a decoupled manner, where each problem is solved separately [24, 23, 20]. In this article, we consider quasi-static droplets, where no internal flow takes place.

The difference between the internal and the external pressure $\triangle p$ on the membrane interface $\mathcal{S}_d$ is balanced by the mean surface curvature $2H$, through the Young-Laplace equation,

$$2H\gamma_{LG} = \triangle p \qquad [\mathrm{N/m^2}], \tag{1}$$

where γ is the surface tension at the liquid-gas interface. The pressure difference across the interface can be expressed as

$$\triangle p = p_f - p_c, \qquad p_f = p_0 + \rho g y, \tag{2}$$

where p_f is the fluid bulk pressure comprising the capillary pressure p_0 and the hydrostatic pressure in terms of the liquid density ρ, gravity g and the surface height y. A contact pressure p_c appears where contact between the membrane and other surfaces take place. Since it is more convenient in computations to use normalized quantities, we multiply Eq.(1) by L/γ_{LG} to obtain the dimensionless quantities marked with tilde,

$$2\tilde{H} = \tilde{p}_f - \tilde{p}_c \qquad [-], \tag{3}$$

$$\tilde{p}_f = \lambda + B_0\,\tilde{y}, \qquad B_0 = \frac{\rho g L^2}{\gamma_{LG}}, \tag{4}$$

where λ is the Lagrange multiplier accounting for the capillary pressure, B_0 is the so called Bond number, and L is a characteristic length, which can be related to the droplet diameter, if it is spherical, or the droplet width otherwise.

2.2 Rigid surface model

Multi-scale surfaces involve multi-level roughness. While a hydrophobic surface is observed to be flat on the macro-scale level, roughness is captured at the meso-scale level, and multi-level roughness at finer length-scales. The mathematical modeling of the substrate surface at three different topographies is presented in this section. These are: flat, single-roughness, and double-roughness topographies (Fig.1), which can be interpreted as three different length-scales. While most authors use simple sinusoidal functions for representation of roughness [4, 13], we

use super-imposed exponential functions, which provide more flexibility in surface description, and better approximation of the real topography. This is because more parameters are used to describe exponential functions. A point $\boldsymbol{x}_m$ on the surface is defined through the relation,

$$\boldsymbol{x}_m = y_1 \boldsymbol{n_0} + y_2 \boldsymbol{n_1}, \tag{5}$$

where $\boldsymbol{n_0}$ and $\boldsymbol{n_1}$ are the normals w.r.t surfaces $\mathcal{S}_0$ (the flat horizontal surface) and $\mathcal{S}_1$, respectively (see Fig.1). The following set of equations describe surfaces of up to two-level roughness,

$$y_1(x_1) = \sum_{j=1}^{n_{p_1}} A_1 \, \exp\Big(- \frac{(x_1 - j\triangle x_1)^2}{h_1^2} \Big), \tag{6}$$

$$y_2(s) = \sum_{j=1}^{n_{p_2}} A_2 \, \exp\Big(- \frac{(s - j\triangle x_2)^2}{h_2^2} \Big), \tag{7}$$

$$s = \int_{\mathcal{S}_1} \sqrt{1 + \Big(\frac{\partial y_1}{\partial x_1}\Big)^2} \, \mathrm{d}x_1. \tag{8}$$

The exponential function y_1 describes the first level of roughness on surface $\mathcal{S}_1$, while y_2 describes the roughness on the second level (surface $\mathcal{S}_2$). The latter is defined in Eq.(7) in terms of the arc length s, measured on surface $\mathcal{S}_1$. A_i and h_i are the amplitude and asperity width of the corresponding surface $\mathcal{S}_i$, respectively, for $i = 1, 2$. A summation over the number of asperities on the corresponding surfaces n_{p_1} and n_{p_1} is taken, considering $\triangle x_1$ and $\triangle x_2$, which define the spacing between asperities on $\mathcal{S}_1$ and $\mathcal{S}_2$, respectively. Setting $A_2 = 0$ yields a single-roughness surface described only by y_1, while setting both $A_1 = A_2 = 0$ yields a flat surface. The width of the asperities on each level is related to a characteristic length L through the relations $h_1 = f_1 L$ and $h_2 = f_2 L$, where $f_1 \& f_2 < 1$ are factors which determine the two length-scales of surface $\mathcal{S}_1$ and $\mathcal{S}_2$, respectively.

In order to describe the roughness, we define the dimensionless surface roughness factor,

$$C_{r_i} = A_i / h_i, \tag{9}$$

which is the ratio of the asperity amplitude to its width on the corresponding surface i. A flat surface would correspond to $C_{r_1} = 0$, while a single-level rough surface correspond to $C_{r_2} = 0$. Furthermore, in this work we fix the distance between each two consequent asperities to three times their width, $\triangle x_i = 3h_i$ for $i = 1, 2$. We emphasize here that both $\triangle x_i$ and h_i are fixed parameters defined in terms of the characteristic length L. In spite of being captured at different length-scales, the two surfaces might have the same roughness factor. Therefore the length-scale is distinguished through the variable h_i and not C_{r_i}.

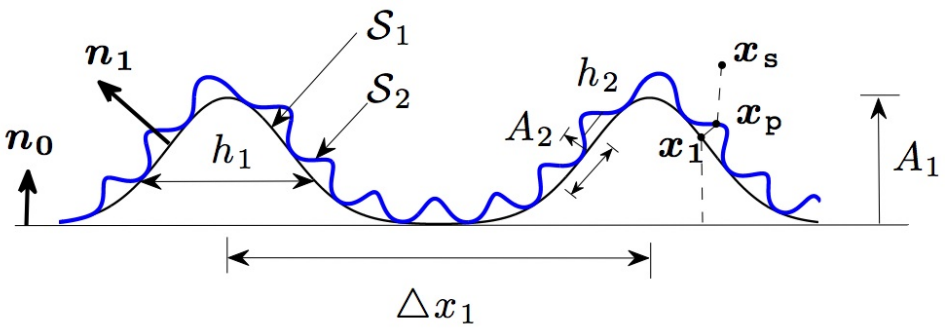

Figure 1: Parameterization of the multi-scale surface.

After defining the droplet and substrate surface models, the numerical treatment of contact is introduced. In order to compute the contact pressure p_c between the droplet membrane surface $\mathcal{S}_d$ and the substrate surface $\mathcal{S}_i$ (Eq.(2)), the normal gap g_n between both surfaces must be computed. For that, each point on the droplet surface is projected normally onto the substrate surface. The impenetrability constraint then reads,

$$g_n = (\boldsymbol{x}_\mathrm{s} - \boldsymbol{x}_p) \cdot \boldsymbol{n}_p \geq 0, \quad \forall\, \boldsymbol{x}_s \in \mathcal{S}_d, \tag{10}$$

where $\boldsymbol{x}_p$ is the closest projection of the membrane point $\boldsymbol{x}_s$ onto the substrate surface $\mathcal{S}_i$ in the direction $\boldsymbol{n}_p$, normal to $\mathcal{S}_i$. Several numerical approaches are introduced by Wriggers [32] to enforce the contact constraint in Eq.(10). While the computation of g_n and its spatial derivatives on a flat surface is straight forward, it is challenging in the case of curved surfaces, since the surface normal varies w.r.t $\boldsymbol{x}_s$. An iterative solution is therefore necessary to compute all possible projection points $\boldsymbol{x}_m$, satisfying the orthogonality condition,

$$\boldsymbol{a}_m \cdot (\boldsymbol{x}_s - \boldsymbol{x}_m) = 0, \tag{11}$$

where $\boldsymbol{a}_m$ is the surface tangent on $\mathcal{S}_i$ at $\boldsymbol{x}_m$. Generally, several projection solutions for $\boldsymbol{x}_s$ could exist, and therefore a minimum distance problem has to be solved to obtain the closest projection point $\boldsymbol{x}_p$,

$$\boldsymbol{x}_p(\boldsymbol{x}_s) = \min_{\forall \boldsymbol{x}_m \in \mathcal{S}_i} (\boldsymbol{x}_s - \boldsymbol{x}_m), \quad \forall\, \boldsymbol{x}_s \in \mathcal{S}_d. \tag{12}$$

In the case of a double-roughness surface, the point $\boldsymbol{x}_p$ on $\mathcal{S}_2$ is computed in terms of the arc length s corresponding to the point $\boldsymbol{x}_1$ on $\mathcal{S}_1$, which is the projection of $\boldsymbol{x}_p$ on $\mathcal{S}_1$.

The three-phase boundary (contact line) changes as the contact area varies, depending on the surface roughness. While most of the literature treat the contact line as a predefined boundary given by Dirichlet boundary conditions, we treat it as an internal interface defined through a force balance based on Young-Dupré equation, where the position is a-priori unknown. The force balance in the tangential and normal directions, respectively, can be written as

$$\gamma_{SG} - \gamma_{LG} \cos\theta_c - \gamma_{SL} = 0, \tag{13}$$

$$q_n - \gamma_{LG} \sin\theta_c = 0, \tag{14}$$

where θ_c is the contact angle measured inside the liquid between the solid and the liquid interfaces, while γ_{SG} and γ_{SL} denote the surface tension at the solid-gas and the solid-liquid interfaces, respectively. q_n is the force which counterbalances the normal component of the surface tension γ_{LG}. Details on the numerical implementation of the contact line can be found in [20] and [26].

3 Model validation

The droplet model is validated experimentally. A convergence study to verify the numerical solution is also provided.

3.1 Validation against experiments

The numerical solution is validated against the experimental solution obtained by Callies et al. [7], and plotted in Fig.2, which depicts an image of an axisymmetric water droplet of given volume V, resting on a flat (observed at the macro-scale) rigid superhydrophobic surface with

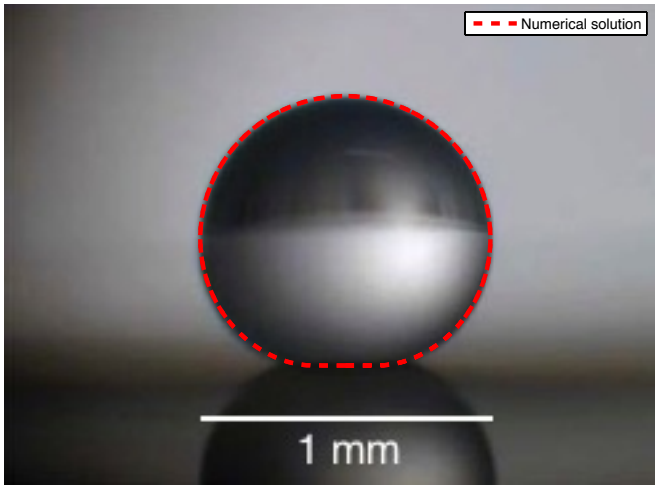

Figure 2: Numerical solution against the experimental solution of Callies et al. [7], for an axisymmetric droplet, $V \approx 0.52$ μl, $\theta_c \approx 180°$. [Adopted with permission from Royal Society of Chemistry, Soft matter, RF14].

($\theta_c \approx 180°$). Droplet parameters are: surface tension $\gamma = 0.0728$ N/m, temperature $20°C$, and density of water $\rho = 998.2$ kg/m^3. The corresponding numerical quantities are Bond number $B_0 = 0.1363$, and the characteristic length $L = 1$mm.

Fig.2 shows good agreement of the numerical solution with experiments for the case of contact on flat surfaces. Furthermore, the experimental solution of Zhang et al. [34] has been considered, and also gave an equally good agreement. Numerical solutions for contact on rough surfaces are verified only numerically in the following subsection.

3.2 Convergence of the numerical solution

Since no analytical solution for a deformed droplet under gravity exists, we study the convergence of the numerical solution based on the relative error computed at each mesh density. This error is defined as the relative difference in the true contact area computed at two consequent mesh densities A^h_{i+1} and A^h_i,

$$\triangle A^h_{true} = \frac{A^h_{i+1} - A^h_i}{A^h_i}, \tag{15}$$

which converges to zero as the number of elements n_{el} goes to infinity (element size goes to zero), as shown in Fig.3. For a very coarse mesh, the error in the true contact area of both flat and rough surfaces is almost identical. This is because the mesh is too course to capture the curved rough surface. Quadratic Lagrange two-dimensional finite elements are used in these computations.

4 Results and discussion

The introduced numerical model can predict the static wetting state on hydrophobic surfaces, based on predefined surface roughness and droplet parameters. Whether it is a Wenzel or Cassie-Baxter wetting state, is therefore a result and not an assumption. As often adopted in

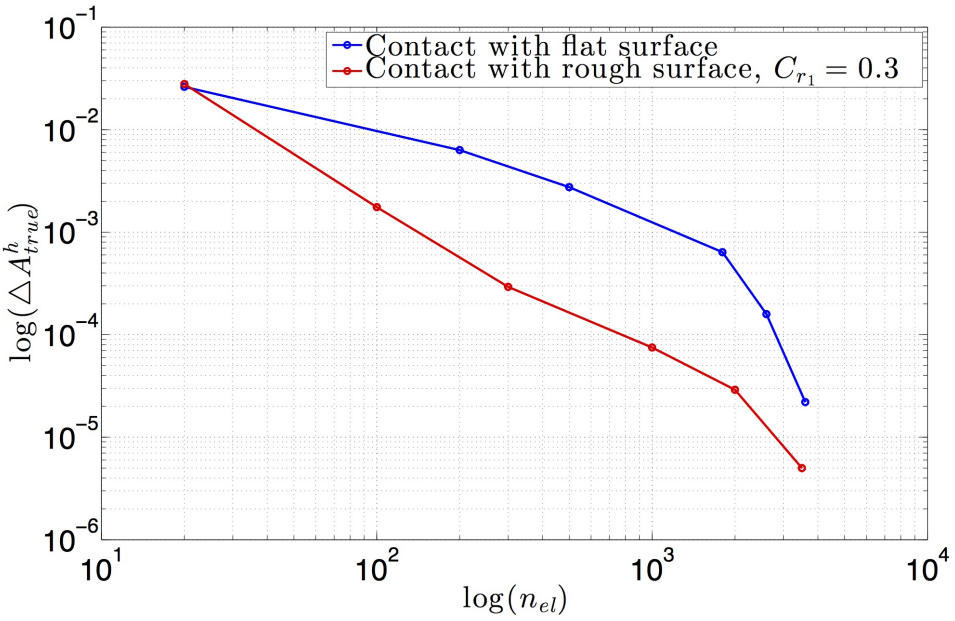

Figure 3: Convergence of the true contact area of a droplet resting on a rigid surface (flat and rough), for $\theta_c = 180°$.

the literature for quasi-static modeling, axisymmetric droplets are considered in this section, so that the 3-D case can be reduced to a simple 2-D model. In fabrication of artificial hydrophobic surfaces, the hydrophobicity is enhanced by minimizing the true contact area, therefore allowing smoother sliding/rolling motion of a droplet on the surface. This minimization can be achieved by: (1) increasing the surface roughness, which results in more air gaps between the droplet and the substrate surface, (2) maximizing the contact angle, and (3) minimizing the droplet size, through chemical or electrical treatments. In order to find local and global minima, an optimization study is necessary, based on predefined constraints. Such a study is not addressed in this article. In this section, we study the effect of these three parameters on: (1) the difference between the true and apparent contact angles ($\theta_{tr} - \theta_{ap}$), and (2) the ratio of the true to apparent contact area (A_{tr}/A_{ap}). The latter can be seen as a quantification of the composite wetting state introduced by Cassie and Baxter [9]. Alternative to A_{tr}/A_{ap}, the surface roughness effect can be studied through the ratio of the true contact area (A_{tr}) to the total surface area of the droplet (A_T) defined as the sum of the true contact area and the free surface area A_f, shown in Fig.4.

While the true contact area A_{tr} and true contact angle θ_{tr} are usually captured at scales smaller than or equal to the micro-scale, where surface roughness appears, the apparent contact area A_{ap} and apparent contact angle θ_{ap} are observed at the macro-scale, where the surface appears flat (see Figs.4 and 5). The dotted line in Fig.5, representing the apparent surface, is chosen to be tangent to the peak of the asperity. θ_{tr} is defined locally at each asperity as the angle between the surface tangents of both the asperity and the droplet surface, at the contact line. This definition is also valid for surfaces with second-level roughness. We note that considering a perfect flat surface, we have $\theta_{tr} = \theta_{ap} = \theta_c$.

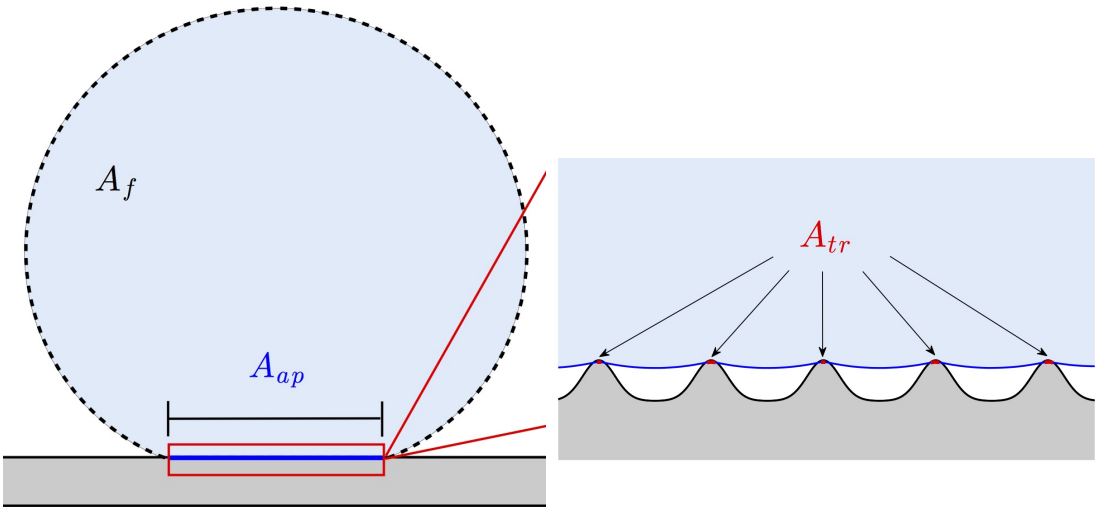

Figure 4: Schematic of true contact area A_{tr}, apparent contact area A_{ap}, and free surface area of the droplet A_f.

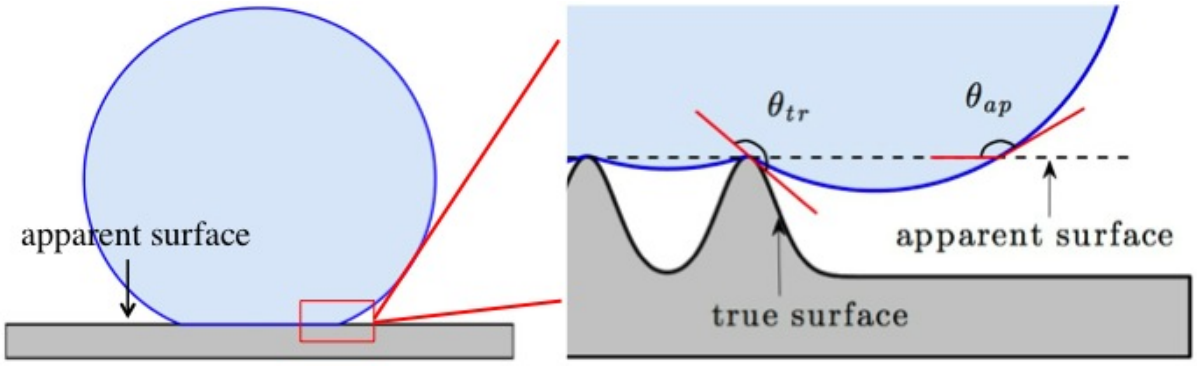

Figure 5: True contact angle θ_{tr} and apparent contact angle θ_{ap}.

4.1 Surface parameters

We investigate the effect of the surface roughness factor C_{r_i} and the true contact angle θ_{tr} on the hydrophobicity. Computations are done for a defined range of contact angles $140^\circ \leq \theta_{tr} \leq 180^\circ$, for a fixed droplet volume V, and fixed spacing between asperities $\triangle x_i = 3h_i$, for $i = 1, 2$. Adaptive finite element meshes are used in the computations, in order to provide finer mesh size in the region of contact and coarser in the region of free surface. The surface roughness factor is chosen in the range $0 \leq C_{r_i} \leq 2$, which covers a reasonable range of surface profiles representing roughness at the length-scales under consideration. Fig.6 shows a droplet with a fixed volume $V = \pi L^3$ in contact with rigid flat and rough surfaces at three different contact angles. On a flat surface, a decrease in the contact angle from 180° to 140° results in a considerable increase in the true contact area (almost four times). In other words, at $\theta_{tr} = 140^\circ$, A_{tr} is 25% of A_T (Fig.6a). This percentage drops to 5.5% in the case of contact with a rough surface of roughness factor $C_{r_1} = 0.9$ (Fig.6b). For computations of contact with flat surfaces in Fig.6, we use 200 quadratic Lagrange finite elements, while for the case of contact with rough surfaces, 2000 quadratic finite elements are used at the contact region.

Fig.7 illustrates the single-level roughness effect on the wetting area. As seen, the ratio A_{tr}/A_{ap} decreases as the surface roughness C_{r_1} increases. Furthermore, curves in Fig.7 have higher

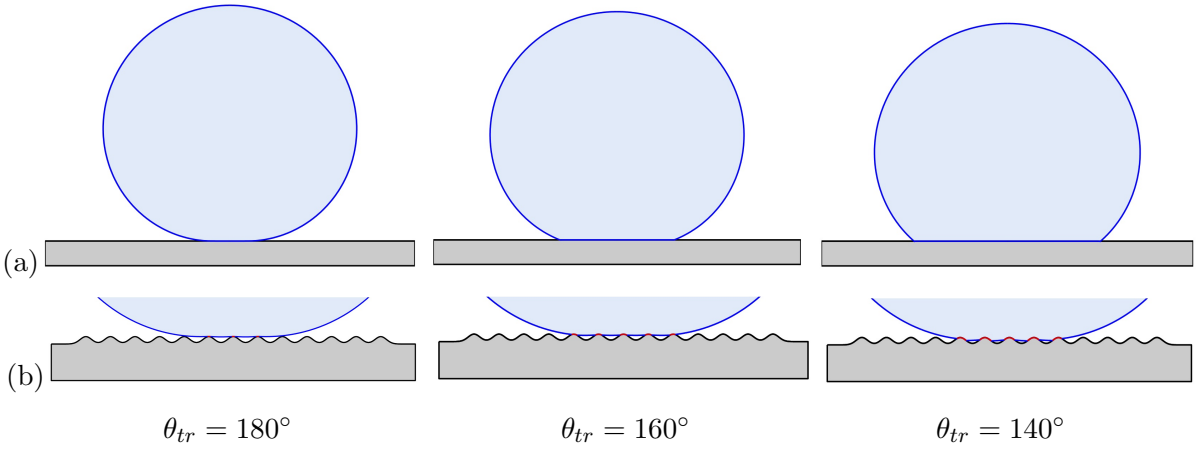

Figure 6: FE solutions for a droplet of volume $V = \pi L^3$, in contact with: a) flat and b) rough surface with $C_{r_1} = 0.9$. True contact angles for both surfaces $=\{180°, 160°, 140°\}$. The ratio of true to total contact area (left to right): (a) A_{tr}/A_T=$\{6.1,\ 15.3,\ 25\}\%$, (b) A_{tr}/A_T =$\{0.9,\ 2.5,\ 5.5\}\%$.

slopes at regions with small roughness factors ($C_{r_1} < 0.4$), and lower slopes at higher roughness factors. This is because the increase of C_{r_1} in the first region correspond to the transition from the non-composite (Wenzel) to the composite contact state (Cassie-Baxter), where the variation in the wetting area (A_{tr}/A_{ap}) is considerably higher than that in the second region where contact is already in a composite state. In the latter state, the droplet is pinned on the asperities of the rough surface. Therefore, with $\triangle x_1$ being fixed, further increase in C_{r_1} would correspond to elevating the droplet, with negligible change in the wetting area. The transition from the Wenzel wetting state (W) to Cassie-Baxter (C-B) state is marked in Fig.7 by the blue lines. This transition occurs at different C_{r_1} as the contact angle changes.

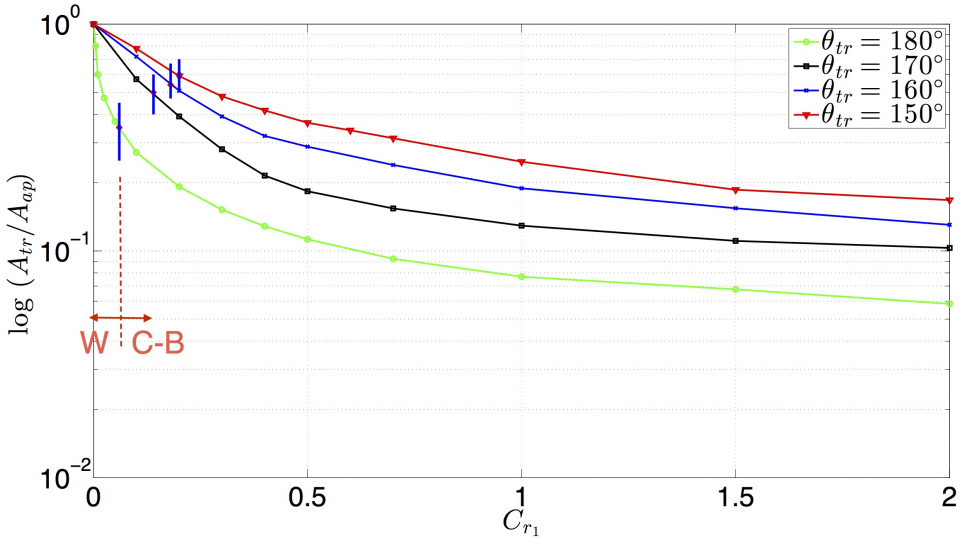

Figure 7: Ratio of true to apparent contact area over surface roughness factor $C_{r_1} = A_1/h_1$, $V = 2\pi L^3$, for a single-roughness surface ($C_{r_2} = 0$).

For a fixed contact angle $\theta_{tr} = 180°$, considering an additional level of roughness, parameterized by the factor C_{r_2}, results in a further decrease in the true contact area, as shown in Fig.8. The roughness factor C_{r_2} here is expressed in terms of C_{r_1} only for simplification, however arbitrary values can also be assigned to the model.

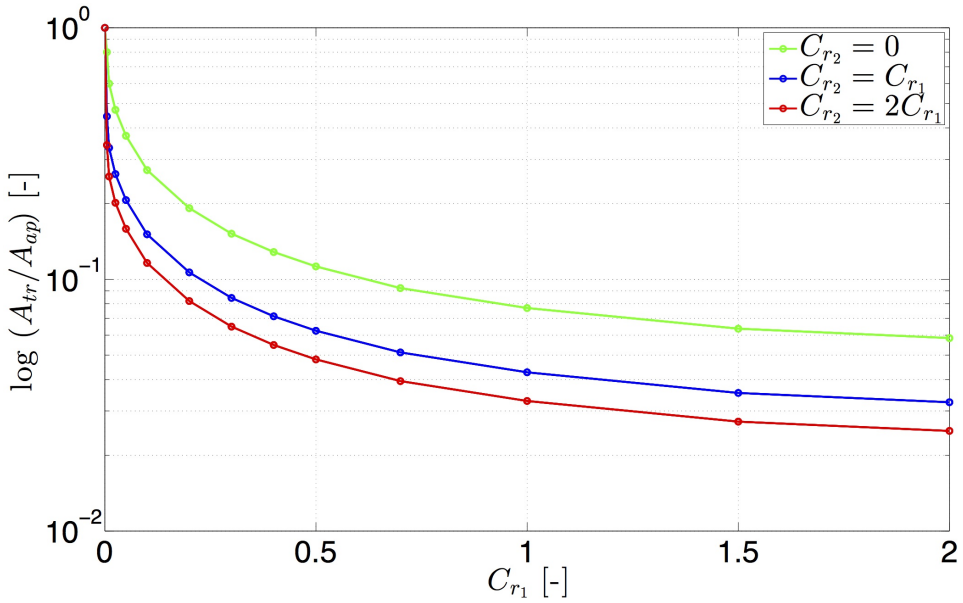

Figure 8: Effect of double-level of roughness on the true to apparent contact area ratio, for $V = 2\pi L^3$, at a fixed contact angle $\theta_{tr} = 180°$.

The second criteria for evaluating the hydrophobicity is the contact angle. For the same droplet volume, larger contact angles result in smaller contact areas (less wetting), as in Fig.7, and smaller differences between the apparent and the true contact angle, as in Fig.9. In analogy to the effect of roughness on the wetting area, the difference $(\theta_{tr} - \theta_{ap})$ increases with a higher slope in the transition region (Cr_1<0.4), compared to the region where contact is already in composite state (Cr_1>0.4).

Fig.10 shows that larger differences between the true and apparent contact angles are observed when a second level of roughness is considered, at a fixed $\theta_{tr} = 180°$.

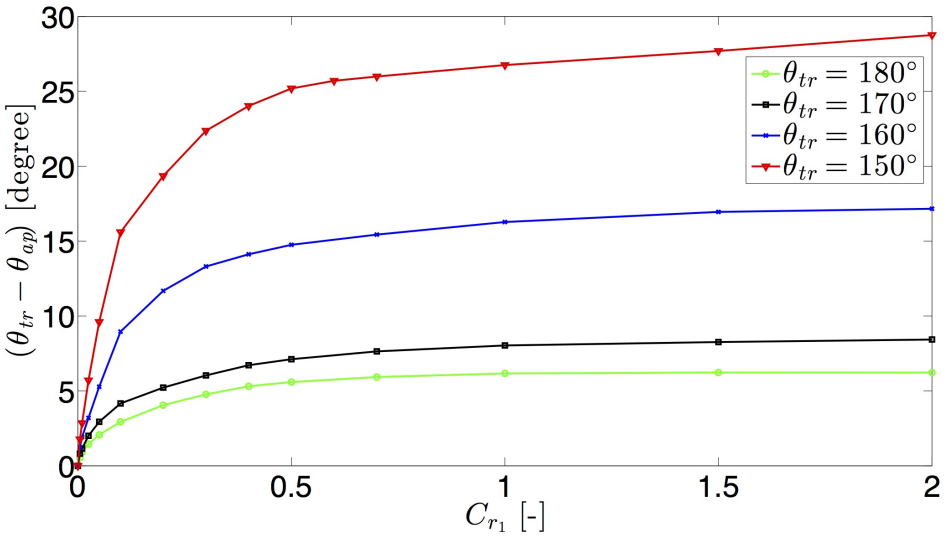

Figure 9: Effect of single-roughness on the true contact angle, $V = 2\pi L^3$, for various θ_{tr}.

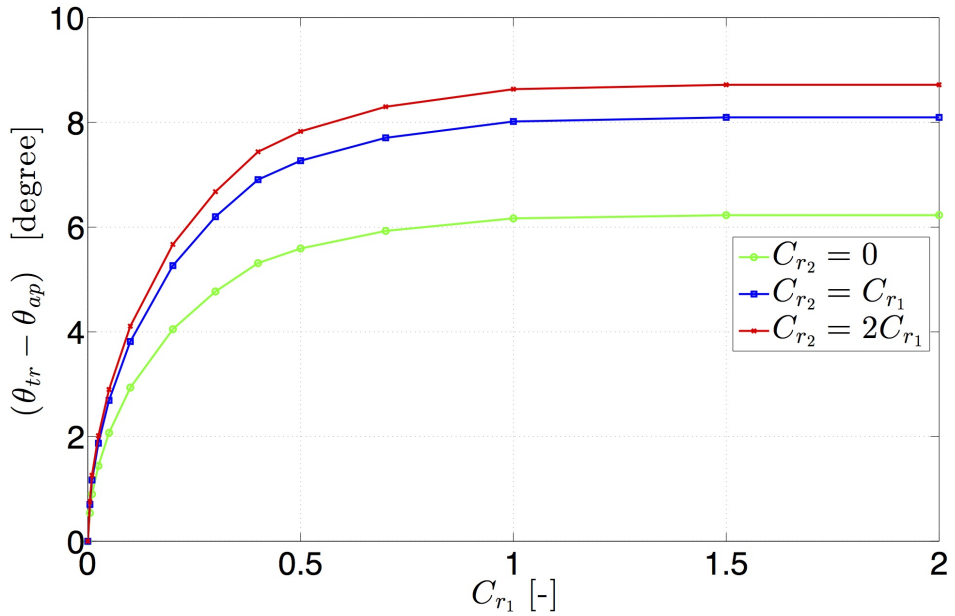

Figure 10: Effect of double-level of roughness on the true to apparent contact angle ratio, $V = 2\pi L^3$, at $\theta_{tr} = 180°$.

4.2 Droplet size

Small droplets of small size have larger surface curvature, and therefore higher capillary pressure, compared to larger droplets. This limits the deformation of a small droplet, as it preserves a semi-spherical shape with a minimum area of contact (see Fig.11). We use the expression size for the volume of an axisymmetric droplet, which is initially a sphere. In 2D, this volume correspond to an area of a circle.

Now, we study the effect of variation of size (i.e volume of an axisymmetric droplet) on the ratio of true contact area to the total droplet area A_{tr}/A_T, at contact angle $\theta_{tr} = 180°$, for single-roughness and flat surfaces. As observed in Fig.12, a linear relationship between the volume and the contact area is obtained for all surfaces, in the defined range of surface roughness and droplet volume. The wetted area increases with the volume at lower slopes for higher surface roughness.

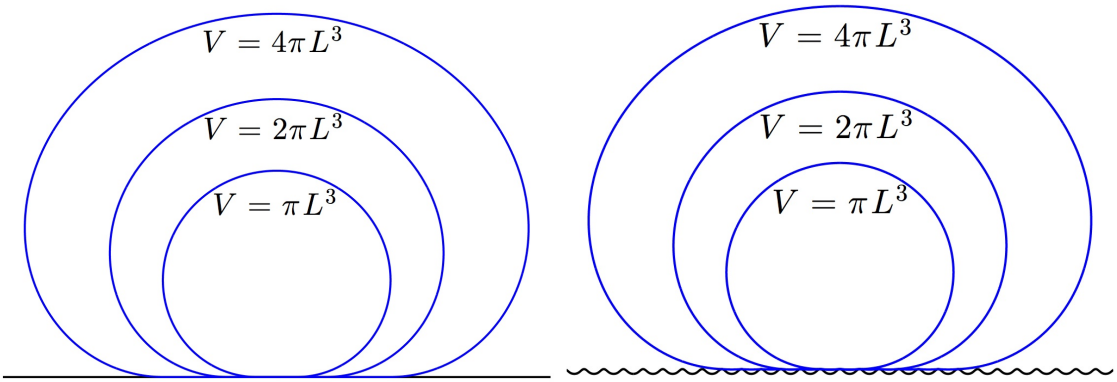

a) b)

Figure 11: Effect of droplet size on the area of contact with (a) flat surface, $C_{r_1} = 0$ and (b) rough surface, $C_{r_1} = 1$.

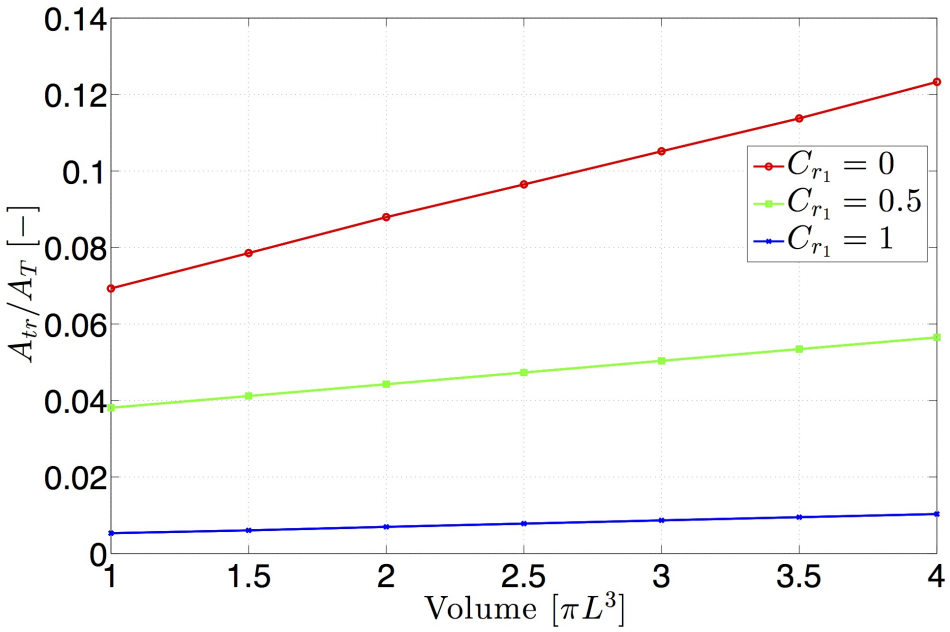

Figure 12: Effect of droplet size on the true to total contact area at different surface roughness factors C_{r_1}, for $\theta_{tr} = 180°$ and $C_{r_2} = 0$.

4.3 Multi-scale representation of hydrophobic surfaces

A multi-scale view of wetting on hydrophobic surfaces is depicted in Fig.13, based on the general surface model discussed in Section 2.2. At smaller scales, where finer asperities are captured on the rough surface, smaller contact area and more air gaps are observed, compared to larger scales. Furthermore, local wetting regions are observed on the single asperities, which differ from the global wetting region observed at larger scales. Therefore considering the multi-scale nature of hydrophobic surfaces provides a realistic modeling of wetting states. The wetting behaviour is highly influenced by the surface and droplet parameters described in previous sections.

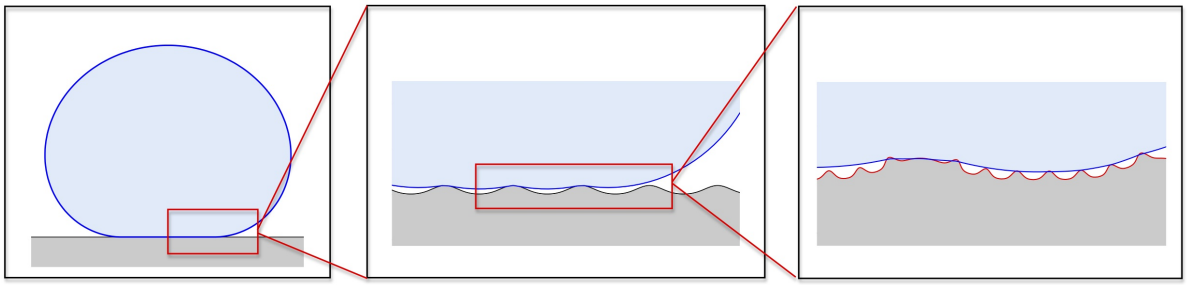

a) b) c)

Figure 13: FE results for a droplet in contact with a super-hydrophobic surface at different length-scales [20], with contact angle $\theta_{tr} = 180°$.

5 Summary and Conclusion

Based on finite element computations, we perform a study on a range of surface and droplet parameters for which the hydrophobicity of rough surfaces is enhanced. This enhancement is mainly achieved by minimization of the wetting area, through manipulating the surface topography, contact angle and the droplet size. The effect of these three parameters on the wetted area is studied.

Three types of surfaces are considered here; flat, single- and double-roughness surface, representing three length-scales: macro-, meso- and micro-scale, respectively. These surfaces are mathematically modeled using super-positioned exponential functions, and parameterized by a surface roughness factor C_r, and a length-scale L. The spacing between asperities is fixed to three times the length-scale. Further study of the effect of this parameter on wetting can be considered in the future. Results show significant changes in the wetted area, as the surface topography changes across different length-scales. Furthermore, true contact angles captured locally at small scales are more precise than the global contact angle measured at a large scale, where the surface appears flat. These conclusions agree with the physical observations of Cassie and Baxter [9], and Lee et al. [16] on the behavior of wetting on rough surfaces. Based on these conclusions, we highlight the importance of considering the surface roughness observed at small length scales while modeling wetting of hydrophobic surfaces. The provided study is specially useful for manufacturing and design of artificial hydrophobic surfaces. Only static wetting is considered in this study. Including inertial effects will result in a different wetting behavior, and therefore different surface design.

Acknowledgements

The authors are grateful to the German Research Foundation (DFG) for the financial support, under grant numbers SA 1822/ 3-2.

References

[1] Agrawal, A. and Steigmann, D. (2009a). Boundary value problems in the theory of lipid membranes. *Continuum Mech. Thermodyn.*, **21**:57–82.

[2] Agrawal, A. and Steigmann, D. (2009b). Modeling protein-mediated morphology in biomembranes. *Biomech. Model Mechanobiol.*, **8**:371–379.

[3] Barthlott, W. and Neinhuis, C. (1997). Purity of the sacred lotus, or escape from contamination in biological surfaces. *Planta*, **202**(1):1–8.

[4] Bittoun, E. and Marmur, A. (2012). The role of multiscale roughness in lotus effect: is it essential for super-hydrophobicity? *Langmuir*, **28**(39):13933–13942.

[5] Brown, R., Orr, F., and Scriven, L. (1980). Static drop on an inclined plate: analysis by the finite element method. *J. Colloid Interface Sci.*, **73**(1):76–87.

[6] Brown, R. and Scriven, L. (1980). The shapes and stability of captive rotating drops. *Philos. Trans. R. Soc. Lond. A*, **297**(1429):51–79.

[7] Callies, M. and Quéré, D. (2012). On water repellency. *Soft Matter*, **1**:55–61.

[8] Carre, A. and Mittal, K. (2009). *Superhydrophobic Surfaces*. VSP/Brill, Leiden.

[9] Cassie, A. and Baxter, S. (1944). Wettability of porous surfaces. *Trans. Faraday Soc.*, **40**:546–551.

[10] ElSherbini, A. and Jacobi, A. (2004). Liquid drops on vertical and inclined surfaces: I. an experimental study of drop geometry. *J. Colloid Interface Sci.*, **273**:556–565.

[11] Ensikat, H., Schutle, A., Koch, K., and Barthlott, W. (2009). Droplets on superhydrophobic surfaces: visualization of the contact area by cryoscanning electron microscopy. *Langmuir*, **25**:13077–13083.

[12] Frstner, R., Barthlott, W., Neinhuis, C., and Walzel, P. (2005). Wetting and self-cleaning properties of artificial superhydrophobic surfaces. *Langmuir*, **21**(3):956–961.

[13] Iliev, S. and Pesheva, N. (2006). Nonaxisymmetric drop shape analysis and its application for determination of local contact angles. *J. Colloid Interface Sci*, **301**:677–684.

[14] Johnson, R. and Dettre, R. (1964). Contact angle, wettability and adhesion. *Adv. Chem. Ser.*, **43**:112–135.

[15] Kavousanakisa, M., Colosquib, C., and Papathanasiou, A. (2013). Engineering the geometry of stripe-patterned surfaces toward efficient wettability switching. *Colloids Surf. A: Physicochem. Eng. Aspects*, **436**:309–317.

[16] Lee, S., Jung, I., and Ko, J. (2008). The effect of the surface wettability of nanoprotrusions formed on network type microstructures. *J. Micromech. Microeng.*, **18**:125007 (7pp).

[17] Ma, M., Hill, R., and Rutledge, G. (2008). A review of recent results on superhydrophobic materials based on micro- and nanofibers. *J. Adhes. Sci. Technol.*, **22**:1799–1817.

[18] Mohammadi, R., Wassink, J., and Amirfazli, A. (2004). Effect of surfactants on wetting of super-hydrophobic surfaces. *Langmuir*, **20**(22):9657–9662.

[19] Onda, T., Shibuichi, S., Satoh, N., and Tsujii, K. (1996). Super-water-repellent fractal surfaces. *Langmuir*, **12**:2125–2127.

[20] Osman, M., R.Rasool, and Sauer, R. A. (2013). Computational aspects of self-cleaning surface mechanisms. In Mittal, K., editor, *Advances in Contact Angle, Wettability and Adhesion*, chapter 7. Wiley.

[21] Raeesi, B., Morrow, N., and G.Mason (2013). Effect of surface roughness on wettability and displacement curvature in tubes of uniform cross-section. *Colloids Surf. A: Physicochem. Eng. Aspects*, **436**:392–401.

[22] Ramiasa, M., Raiston, J., Fetzer, R., and Sedev, R. (2014). The influence of topography on dynamic wetting. *Adv Colloid Interface Sci.*, **206**:275293.

[23] Rasool, R., Osman, M., and Sauer, R. (2013). Computational modeling of liquid droplets moving on rough surfaces. *Proc. Appl. Math. Mech.*, **13**(1):233234.

[24] Rasool, R., Sauer, R. A., and Osman, M. (2012). Internal flow analysis for slow moving small droplets in contact with hydrophobic surfaces. *Proc. Appl. Math. Mech.*, **12**:489–490.

[25] Sas, I., Gorga, R., Joines, J., and Thoney, K. (2012). Literature review on superhydrophobic self-cleaning surfaces produced by electrospinning. *J. Polym. Sci., B: Polym. Phys.*, **50**(12):824–845.

[26] Sauer, R. (2014). Stabilized finite element formulations for liquid membranes and their application to droplet contact. *Int. J. Numer. Meth. Fluids*, **75**(7):519–545.

[27] Sauer, R., Duong, X., and Corbett, C. (2014). A computational formulation for constrained solid and liquid membranes considering isogeometric finite elements. *Comput Method Appl Mech Engrg*, **271**:48–68.

[28] Sommers, A. and Jacobi, A. (2006). Creating micro-scale surface topology to achieve anisotropic wettability on an aluminum surface. *J. Micromech. Microeng.*, **16**:1571–1578.

[29] Steigmann, D., Baesu, E., Rudd, R., Belak, J., and McElfresh, M. (2003). On the variational theory of cell-membrane equilibria. *J. Interfaces Free Bound.*, **5**:357–366.

[30] Suzuki, S., Nakajima, A., Sakai, M., Sakurada, Y., Yoshida, N., Hashimoto, A., Kameshima, Y., and Okada, K. (2008). Slipping and rolling ratio of sliding acceleration for a water droplet sliding on fluoroalkylsilane coatings of different roughness. *Chem. Lett.*, **37**(1):58–59.

[31] Wenzel, R. (1936). Resistance of solid surfaces to wetting by water. *Ind. Eng. Chem.*, **28**:988–994.

[32] Wriggers, P. (2006). *Computational Contact Mechanics*. Springer, 2^{nd} ed.

[33] Young, T. (1805). An essay on the cohesion of fluids. *Phil. Trans. R. Soc. Lond. 95*, **65**.

[34] Zhang, X., Shi, F., Niu, J., Jiang, Y. G., and Wang, Z. Q. (2008). Superhydrophobic surfaces: from structural control to functional application. *J. Mater. Chem.*, **18**:621–633.